

# A simplified focusing and astigmatism correction method for a scanning electron microscope

Yihua Lu, Xianmin Zhang,<sup>a</sup> and Hai Li

*Guangdong Provincial Key Laboratory of Precision Equipment and Manufacturing Technology,  
School of Mechanical and Automotive Engineering, South China University of Technology,  
510640 Guangzhou, China*

(Received 18 October 2017; accepted 10 January 2018; published online 22 January 2018)

Defocus and astigmatism can lead to blurred images and poor resolution. This paper presents a simplified method for focusing and astigmatism correction of a scanning electron microscope (SEM). The method consists of two steps. In the first step, the fast Fourier transform (FFT) of the SEM image is performed and the FFT is subsequently processed with a threshold to achieve a suitable result. In the second step, the threshold FFT is used for ellipse fitting to determine the presence of defocus and astigmatism. The proposed method clearly provides the relationships between the defocus, the astigmatism and the direction of stretching of the FFT, and it can determine the astigmatism in a single image. Experimental studies are conducted to demonstrate the validity of the proposed method. © 2018 Author(s). All article content, except where otherwise noted, is licensed under a Creative Commons Attribution (CC BY) license (<http://creativecommons.org/licenses/by/4.0/>). <https://doi.org/10.1063/1.5009683>

## I. INTRODUCTION

A scanning electron microscope (SEM) is a microscope that produces images by scanning the surface of sample with a focused beam of electrons.<sup>1</sup> Because of the advantages of high resolution, SEMs are widely used in material science for components measurement.<sup>2–4</sup> Recently, in the area of Micro/Nano manipulation, with the urgent demand for high-resolution sensors, SEM has been used as a global sensor for tracking the handling tools and objects to realize automatic manipulation.<sup>5–8</sup> For example, based on visual feedback and force feedback, Fatikow et al.<sup>9–11</sup> performed a series of Micro/Nano tasks involving carrying and placing silica balls of diameter of 1160nm, 519nm and 237nm automatically in the corresponding size hole. In addition, Ru et al.<sup>12</sup> developed the classic four-point probe measurement system and realized automated measurement of nanowires inside the SEM. In this system, the end-effector in the SEM images is used as a feedback and is tracked, and focus and astigmatism must be adjusted regularly during the continuous image acquiring process.

Actually, in most applications of SEM, focus and astigmatism must be accurately adjusted, especially for applications where dimension measurement is involved. However, focusing and astigmatism correction are difficult and time-consuming, even for the professional operators, in practice.<sup>13</sup>

Recently, several automatic focusing and astigmatism correction methods have been developed, most of which are performed based on gradient analysis<sup>14–18</sup> or the power spectrum.<sup>13,19,20</sup> For example, to achieve focusing, Burge et al.<sup>17</sup> maximized the sum of the squared differences between neighboring points over the whole image, and Tee et al.<sup>18</sup> maximized the sum of the intensity gradient magnitudes. However, methods based on gradient analysis are sensitive to noise;<sup>13</sup> to overcome this drawback, methods based on the power spectrum have been investigated. For example, Erasmus and Smith<sup>19</sup> detected astigmatism from the asymmetry of the power spectrum using an on-line computer system and digital frame storage. It is capable of setting focus and correcting astigmatism at least as

---

<sup>a</sup>E-mail: [zhangxm@scut.edu.cn](mailto:zhangxm@scut.edu.cn)

accurately as can be achieved by an experienced operator, but it is only valid for a rather limited class of specimen. Jae Hyung Ahn et al.<sup>20</sup> developed an algorithm to correct astigmatism and defocus, in which a Gaussian function is used to approximate the point spread function to represent the current distribution of the electron beam, and Fourier transformation and least area ellipse fitting are introduced to calculate the radii of the major and minor axes of the ellipse; in order to obtain clear images, it needs to compare images and to adjust focus and astigmatism when it corrects astigmatism. However, these power spectrum based studies require at least two images to determine the astigmatism by comparing these images, and they cannot explicitly provide the relationships between defocus, astigmatism and the direction of stretching of the FFT. Accordingly, in this paper, we will focus on the influence of defocus and astigmatism on the direction of stretching of the FFT, and propose a simplified algorithm that corrects defocus and astigmatism based on FFT and ellipse fitting. A distribution map is proposed to determine the astigmatism using only one image. Different from other methods, the proposed method first corrects astigmatism and then correct defocus; this approach makes the process clearer. Experiments are conducted to demonstrate the performance of the proposed method.

The remainder of this paper is organized as follows. Section II-A starts with the description and the basic principle of the defocus and astigmatism, and provides the influence of defocus and astigmatism on the direction of stretching of the FFT (distribution map); section II-B describes the astigmatism correction algorithm using FFT and ellipse fitting. Experiments are conducted in Section III to demonstrate the practicability of the proposed algorithm, and section IV concludes this paper.

## II. METHODOLOGY

### A. Influence of defocus and astigmatism on the FFT

When an image is in-focus and has no astigmatism, the high-energy electron beam forms a single point on the surface of the specimen, as illustrated in figure 1(a), and it has the smallest spot size, thereby achieving clear imaging, as illustrated in figure 1(d). When an image is defocused, the electron beam no longer forms a single point but a round spot, and the image is blurred, as shown in figure 1(b) and figure 1(e). When the image has astigmatism, the spot formed by the electron beam is stretched in one direction, i.e., the spot is an elliptical spot, as illustrated in figure 1(c) and figure 1(f).

Thus, the following six factors affect the clarity of images (individually or in combination): Over focus (defined as F+), Under focus (defined as F-), stigma X increased (defined as X+), stigma X decreased (defined as X-), stigma Y increased (defined as Y+) and stigma Y decreased (defined as Y-).

Different combinations of defocus and astigmatism lead to different directions of stretching of the spot. The proposed method involves generation of a distribution map that explicitly provides the influence of defocus and astigmatism on the direction of stretching of the FFT image, as shown in figure 2. Based on the distribution map, only one image is required to determine the astigmatism present in the system, whereas two images are required for other methods.

### B. Correction algorithm

An algorithm is developed to achieve focusing and astigmatism correction. The [supplementary material](#) shows the detailed flow charts of the algorithm.

The SEM is equipped with a precision X/Y/Z triaxial sample platform. The algorithm starts by storing the Z-axis position of the sample platform, the current focal length value and the current astigmatism value. By comparing the Z-axis position of the sample platform and the current focal length, the Z-axis position of the sample platform is adjusted to achieve a coarse positioning of the focus.

At the beginning, FFT of the SEM image is first conducted; the following formula is used for the FFT:

$$h = n \log(1 + m) \quad (1)$$

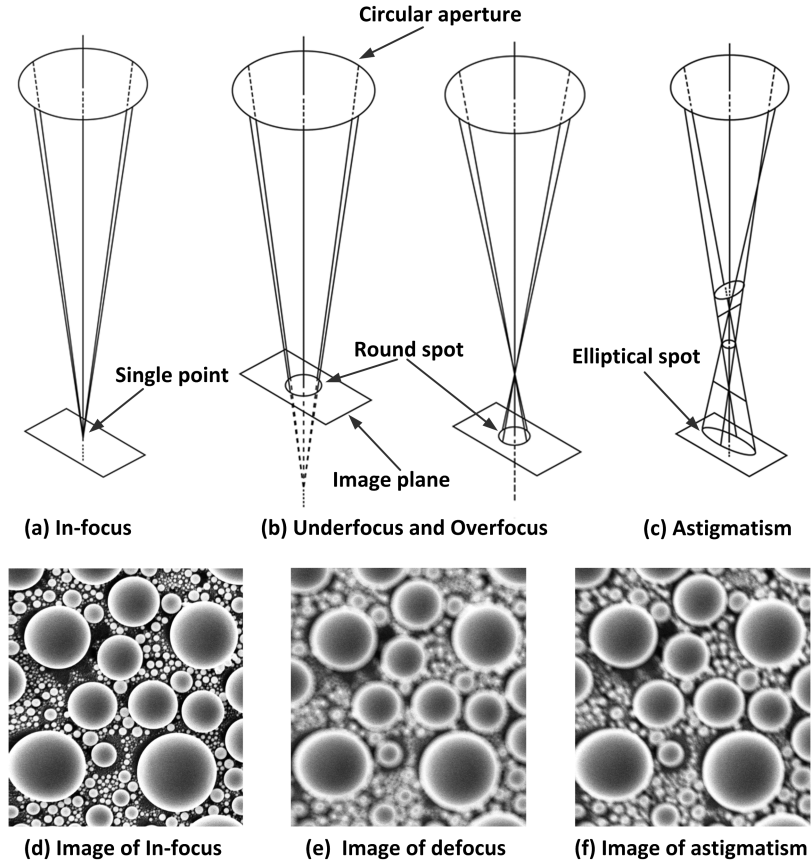


FIG. 1. Diagram illustrating the formation of images.

where  $h$  is the final value of the pixel,  $n$  is a scaling constant, and  $m$  is the gray value of a pixel of the FFT.

The FFT of the SEM image is subsequently processed using a threshold with a value of 150, which is determined experimentally to achieve a suitable result in this work. By threshold processing, pixels with gray value less than 150 are displayed as black (intensity 0), whereas pixels with gray value greater than or equal to 150 are displayed as white (intensity 255). The result is that most high-frequency components are removed, leaving the low-frequency components, as illustrated in figure 3.

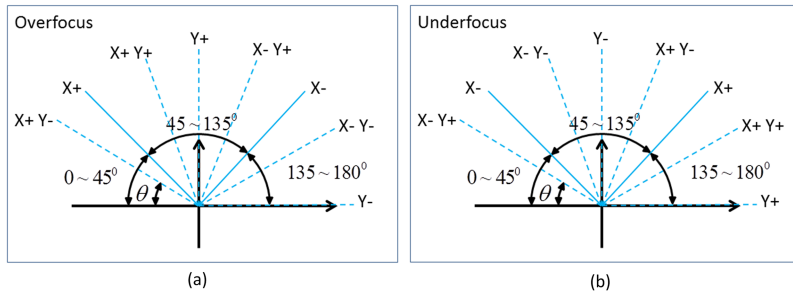


FIG. 2. The influence of defocus and astigmatism on the direction of stretching of the FFT. (a) the direction of stretching when the SEM system is over focus and under different astigmatism; (b) the direction of stretching when the SEM system is under focus and under different astigmatism.

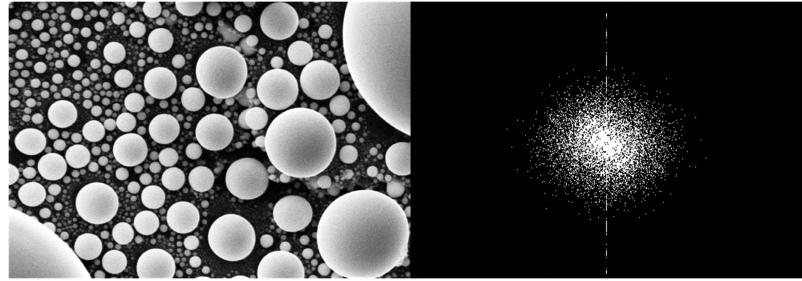


FIG. 3. Images of tin-on-Carbon sample and its fast Fourier transform (In-focus and no astigmatism).

Subsequently, the pixels of the threshold FFT are used for ellipse fitting. The threshold FFT is stretched in one direction by the combination of defocus and astigmatism; as a result, the pixels form an obvious elliptical shape. The steps of the ellipse fitting of threshold FFT pixels are as follows:

First, a pixel with a number of pixel in the neighborhood of less than a certain number is considered as an isolated point and is removed; second, a coordinate system is established on the threshold FFT, as illustrated in figure 4, and the pixels are used for ellipse fitting using the least square method.<sup>21,22</sup> The elliptic formula is fitted as follows:

$$Ax^2 + Bxy + Cy^2 + Dx + Ey + F = 0 \quad (2)$$

Each coefficient is determined by calculating the minimum value of the following function:

$$f(A, B, C, D, E, F) = \sum_{i=1}^n (Ax_i^2 + Bx_iy_i + Cy_i^2 + Dx_i + Ey_i + F)^2 \quad (3)$$

That is, by calculating the following formula's linear equations:

$$\frac{\partial f}{\partial A} = \frac{\partial f}{\partial B} = \frac{\partial f}{\partial C} = \frac{\partial f}{\partial D} = \frac{\partial f}{\partial E} = \frac{\partial f}{\partial F} = 0 \quad (4)$$

Each coefficient is determined using the Gaussian elimination method,<sup>23,24</sup> and then the elliptical equation is obtained.

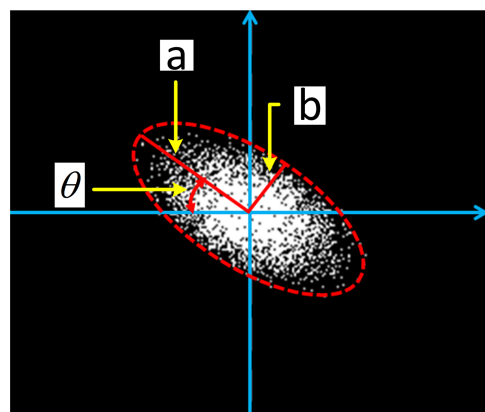


FIG. 4. Coordinate system established on the threshold FFT.

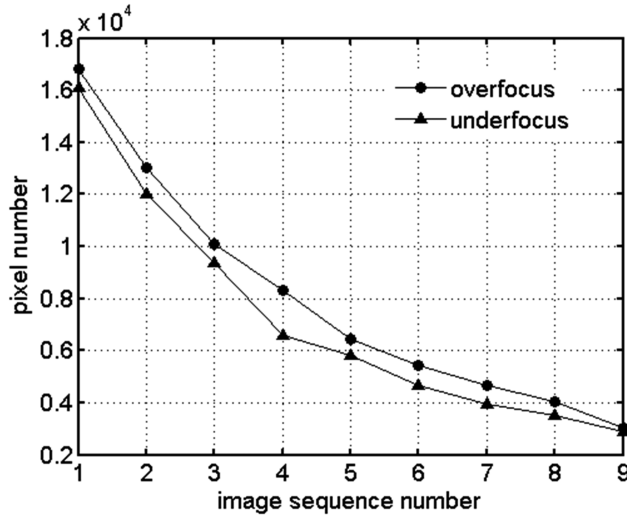


FIG. 5. Pixels number of threshold FFT sequence. The first image is the most clear and the last image is the most blurred.

Third, the elliptic parameters, such as semi major axis (defined as  $a$ ), semi minor axis (defined as  $b$ ), and ellipse azimuth (defined as  $\theta$ ), are calculated as follows:

$$\begin{cases} a = 2 \times \sqrt{\frac{-2F}{A + C - \sqrt{B^2 + \left(\frac{A-C}{F}\right)^2}}} \\ b = 2 \times \sqrt{\frac{-2F}{A + C + \sqrt{B^2 + \left(\frac{A-C}{F}\right)^2}}} \\ \theta = 180 - \frac{1}{2} \arctan \left( \frac{F}{A - C} \right) \end{cases} \quad (5)$$

The elliptic parameters are used to first correct the X astigmatism and then correct the Y astigmatism. Based on the distribution map (figure 2), the astigmatism present in the system can be determined using one threshold FFT. Thus, astigmatism correction can be performed as follow:

Adjust stigma X to correct X astigmatism until  $\theta$  is close to  $0^\circ$  or  $90^\circ$  (a deviation of  $\alpha$  is possible), which implies X astigmatism is corrected.

Adjust stigma Y to correct Y astigmatism until  $\frac{|a-b|}{a} < t$ , which implies Y astigmatism is corrected.

After the astigmatism is corrected, only defocus must be corrected. The number of pixels of the threshold FFT is statistically calculated, as illustrated in figure 5. By adjusting the focus length, the sample is in the focal length when the number of pixels reaches the maximum.

### III. EXPERIMENT VERIFICATION AND DISCUSSION

The SEM used in this work is a Carl ZEISS EVO MA-15 instrument. The adjustment of the final lens is used to change the focal length and achieve a working distance from 0 mm to more than 40 mm. Electromagnetic stigmators are used to correct astigmatism by providing a quadrupole field to correct the beam ellipticity.<sup>25</sup> Astigmatism can be corrected by adjusting the stigma X and stigma Y controls on the SEM. Each stigma controls the magnitude and direction of the current through the coils.

Two experiments are conducted to demonstrate the practicability of the method. The first experiment is employed to show the veracity of the distribution map with defocus and astigmatism; the second experiment is conducted to verify the performance of the algorithm.

### A. Verification of the distribution map

A tin-on-carbon sample is employed to verify the influence of defocus and astigmatism on the direction of stretching of the FFTs. In this experiment, the tin-on-carbon sample is chosen mainly because its FFT is close to round symmetry. A series of images with different combinations of defocus and astigmatism are captured, and their FFTs are processed via a threshold using a value of 150, as illustrated in figure 6 and figure 7.

The threshold FFTs are used for ellipse fitting and are stretched in one direction by the combination of defocus and astigmatism; the ellipse azimuth  $\theta$  are shown in Table I for  $t=12\%$ . From the results, a deviation of approximately  $\pm 5^0$  of the direction of stretching is found because of the non-circular symmetry of tin-on-carbon's FFTs, in agreement with the distribution map. Thus, the astigmatism of the system in the current state can be determined by the distribution map using one image, such capability is not provided by the other methods.

Note that the algorithm can be more accurate if there is a reference sample for which the FFT is closer to round symmetry after focusing and astigmatism correction. In other words, if there is a sample that can achieve  $\frac{|a-b|}{a} < t$  (for  $t < 5\%$  or even  $t < 3\%$ ) after focusing and astigmatism correction, then it is an ideal sample for astigmatism correction and can achieve a better result.

### B. Performance of the algorithm

Experiments are conducted to verify the performance of the algorithm. Figure 8 shows some other images and their FFTs before and after running the algorithm. The SEM system is first set to under focus; according to the distribution map, it can be seen that there are X+ astigmatism and

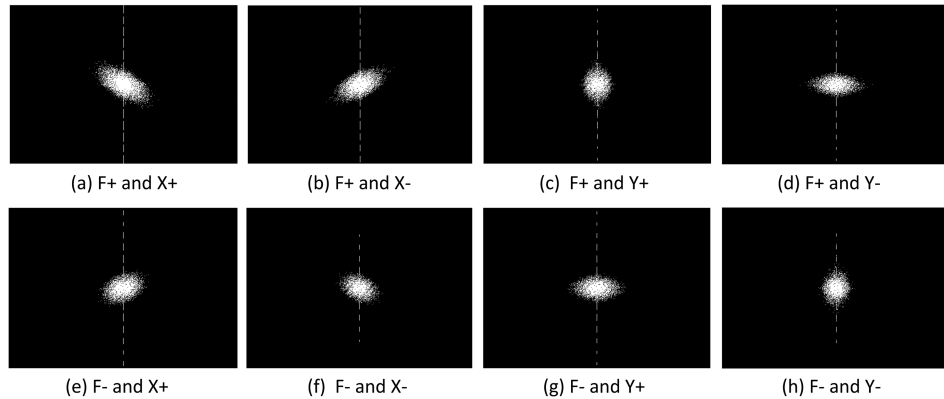


FIG. 6. FFTs of tin-on-Carbon sample under different combinations of defocus and astigmatism (two factors).

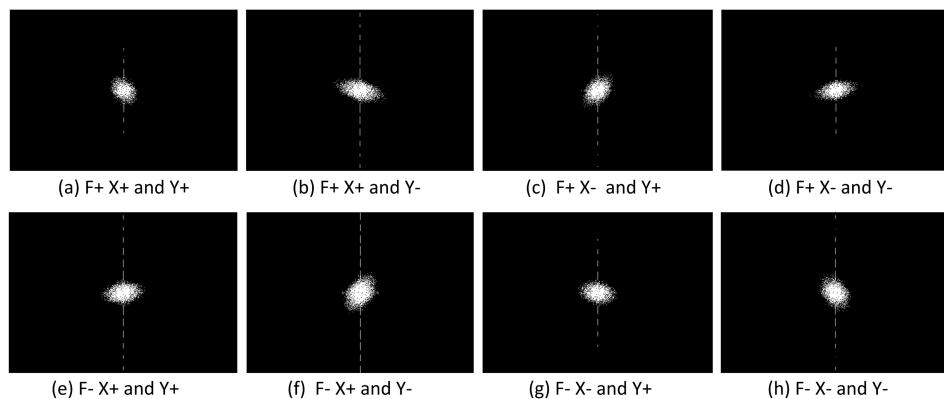


FIG. 7. FFTs of tin-on-Carbon sample under different combinations of defocus and astigmatism (three factors).

TABLE I. Combinations of defocus and astigmatism and their corresponding theoretical value and actual value of  $\theta$ .

No.	Factors	Theoretical value of $\theta$	Actual value of $\theta$	No.	Factors	Theoretical value of $\theta$	Actual value of $\theta$
1	F+ X+	45	40.26	9	F+ X+ Y+	45~90	47.75
2	F+ X-	135	138.95	10	F+ X+ Y-	0~45	13.86
3	F+ Y+	90	87.23	11	F+ X- Y+	90~135	132.46
4	F+ Y-	0	2.48	12	F+ X- Y-	135~180	168.35
5	F- X+	135	139.49	13	F- X+ Y+	135~180	173.68
6	F- X-	45	40.31	14	F- X+ Y-	90~135	132.53
7	F- Y+	0	1.83	15	F- X- Y+	0~45	19.47
8	F- Y-	90	92.73	16	F- X- Y-	45~90	47.38

Y+ astigmatism in figure 8(a). Thus, both stigma X and stigma Y should be decreased to eliminate the astigmatism. The azimuth  $\theta$  is close to  $180^\circ$  ( $0^\circ$ ) after the X+ astigmatism is eliminated, as illustrated in figure 8(b); the FFT become round after the Y+ astigmatism is eliminated, as illustrated in figure 8(c). Figure 8(d) shows the final result after focusing; the result is good enough to perform the follow-up analysis and processing. Figure 9 shows how the focus and stigma values change as the algorithm corrects the image in figure 8(a); it can be seen that the defocus and astigmatism can be corrected in few iterations.

To accommodate different samples, the tin-on-carbon and other samples containing directional features are mounted on the sample platform simultaneously, with the tin-on-carbon used as the reference sample; the FFT of the image of the reference sample is used to correct the astigmatism of the SEM system. Afterwards, the sample to be observed is moved to the high-energy electron beam via the motion of the sample platform; this translation results in the system being defocused because of the different heights between the reference sample and the sample to be observed.

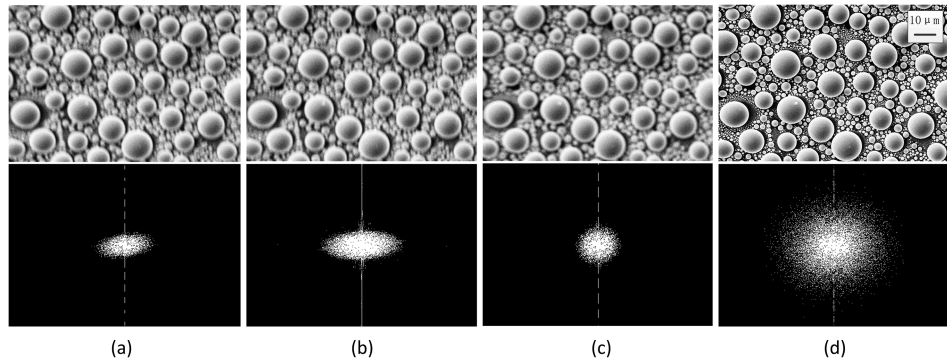


FIG. 8. Tin-on-carbon images and their FFTs before and after running the algorithm.(a) image and its FFT with astigmatism and under focus; (b) image and its FFT after X+ astigmatism is eliminated; (c) image and its FFT after Y+ astigmatism is eliminated; (d) image and its FFT after focusing.

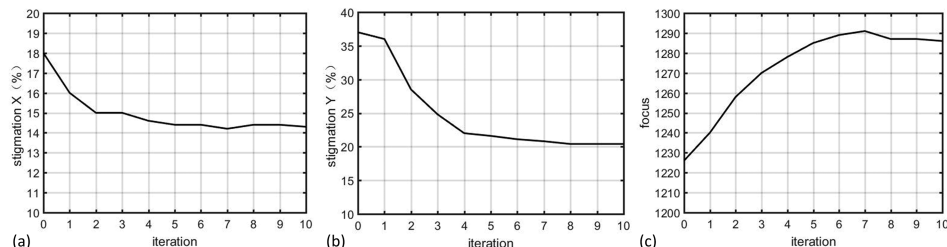


FIG. 9. Various plots when the algorithm is run to correct the image in figure 8(a). (a) plot of stigmatism X against iteration; (b) plot of stigmatism Y against iteration; (c) plot of focus against iteration.

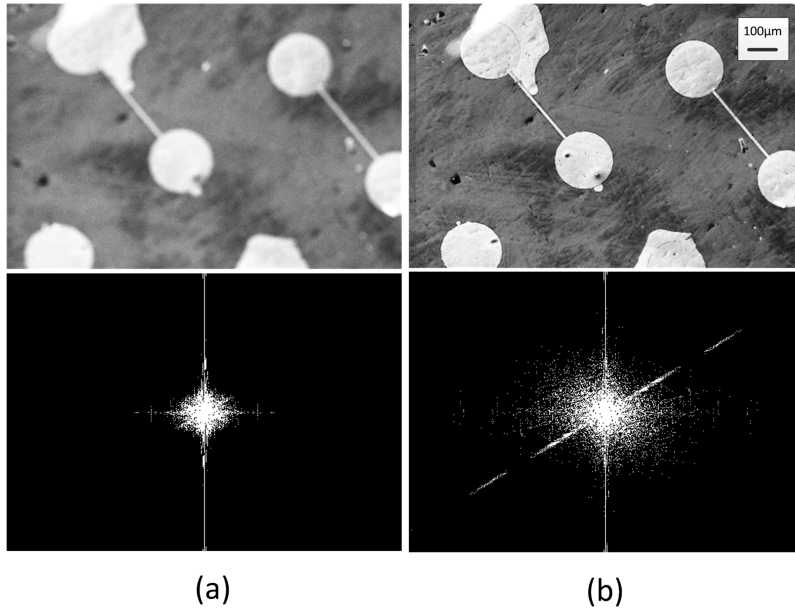


FIG. 10. Sample containing directional features. (a) image and its FFT before focusing; (b) image and its FFT after focusing.

After running the focusing function of the proposed algorithm, the very clear imaging results are obtained, as illustrated in figure 10(b), the clear edge of the feature can be seen and it can be determined whether there is disconnection.

Finally, to verify the effectiveness of the proposed method, a standard calibration board (AGS1932) obtained from Agar Scientific is utilized. The feature nominal length of the calibration board is 10 microns and the height between raised structure and concave structure is very small.

Three groups of images were captured, with 10 images in each group. The experimental study is described as follows. First, the system is set to be defocus, and a group of defocused images of the calibration board is captured. Second, the proposed method is implemented to correct the defocus; after that, the second group of focused images is captured. Third, the system is set to be defocus again, and another group of focused images is captured after manually correcting the defocus by a SEM professional operator. Finally, all of the three groups of images are processed with the same procedure by using Gaussian smoothing and edge extraction.

The feature size in the center of the imaging area is measured after edge extraction, as illustrated in figure 11. The results are shown in Table II. By using the proposed method, an average size of 9.831 microns and a standard deviation of 0.012 are obtained; this result indicates a higher stability of the proposed method since it has a smaller standard deviation and closer to the nominal length of

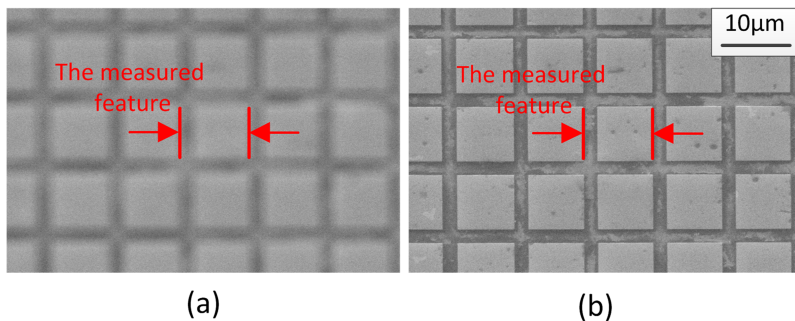


FIG. 11. A calibration board before and after focusing. (a) a defocus image of calibration board; (b) a focusing image of calibration board.

TABLE II. Measurement results of the feature of the calibration board.

No.	feature size ( $\mu\text{m}$ ) (before automatic correction)	feature size ( $\mu\text{m}$ ) (after automatic correction)	feature size ( $\mu\text{m}$ ) (manual focus)
1	9.776	9.851	9.835
2	9.864	9.814	9.853
3	9.833	9.823	9.827
4	9.811	9.825	9.812
5	9.827	9.837	9.822
6	9.807	9.818	9.819
7	9.785	9.828	9.821
8	9.761	9.852	9.831
9	9.817	9.837	9.824
10	9.782	9.824	9.859
Average size	9.806	9.831	9.830
Standard deviation	0.029	0.012	0.014

the feature. In addition, the results obtained by using the proposed method have comparable feature size and standard deviation with that obtained by using manual correction method. These indicate that the proposed method can obtain images as clear as an experienced operator can, but with less time consuming.

#### IV. CONCLUSIONS

This paper presents a practical method for defocus and astigmatism correction of a SEM based on FFT and ellipse fitting. The proposed algorithm clearly provides the relationship between the defocus, the astigmatism and the ellipse azimuth of the FFT, and it can determine the astigmatism of the system using only one image. Experiments were conducted that demonstrated the capability of the proposed method to correct defocus and astigmatism. Different from other algorithms, the proposed method first corrects astigmatism and then corrects defocus, making the method simplified and intuitive. The proposed method can be used as a basis for automated defocus and astigmatism correction in automated Micro/Nano manipulation and deliver a satisfactory performance.

#### SUPPLEMENTARY MATERIAL

See [supplementary material](#) for the detailed flow charts of the algorithm.

#### ACKNOWLEDGMENTS

This work was supported by the National Natural Science Foundation of China (Grant Nos. U1501247, U1609206), the Natural Science Foundation of Guangdong Province (Grant No. 2015A030310278) and the Scientific and Technological Project of Guangzhou (Grant No. 2015090330001). These supports are greatly acknowledged.

<sup>1</sup> D. Zhang, *SEM and EDS technology* (South China University of Technology Press, Guangzhou, 2009) p. 13.

<sup>2</sup> L. H. Lang, Q. D. Zhang, Z. Y. Sun, and Y. Wang, "Analysis of the flow property of aluminum alloy AA6016 based on the fracture morphology using the hydroforming technology," *AIP Advances* **7**(9), 235–243 (2017).

<sup>3</sup> J. Iqbal, T. Jan, S. UI-Hassan, I. Ahmed, Q. Mansoor *et al.*, "Facile synthesis of Zn doped CuO hierarchical nanostructures: Structural, optical and antibacterial properties," *5*(12), 122–127 (2015).

<sup>4</sup> S. Fatikow, V. Eichhorn, F. Krohs, I. Mircea, C. Stolle, and S. Hagemann, "Development of automated microrobot-based nanohandling station for nanocharacterization," *Microsyst. Technol.* **14**, 463–474 (2008).

<sup>5</sup> T. Fukuda, F. Arai, and M. Nakajima, "*Micro-nanorobotic manipulation systems and their applications*," Berlin, Heidelberg: 2013.

<sup>6</sup> L. Dong, F. Arai, and T. Fukuda, "3D nanorobotic manipulation of nano-order object inside SEM," 2000 International symposium on micromechatronics and human science:2000.

<sup>7</sup> Y. Shen and T. Fukuda, "State of the art: Micro-nanorobotic manipulation in single cell analysis," *Robotics and Biomimetics* **1**(21), 152–165 (2014).

<sup>8</sup> H. Xie and S. Regnier, "Development of a flexible robotic system for multiscale applications of micro/nanoscale manipulation and assembly," *IEEE/ASME Transactions on Mechatronics* **16**(2), 266–276 (2011).

- <sup>9</sup> T. Tiemerding, S. Zimmermann, and S. Fatikow, "Robotic dual probe setup for reliable pick and place processing on the nanoscale using haptic devices," 2014 IEEE/RSJ International Conference on Intelligent Robots and Systems, 14–18, 2014, Chicago, IL, USA.
- <sup>10</sup> S. Zimmermann, T. Tiemerding, and S. Fatikow, "Automated robotic manipulation of individual colloidal particles using vision-based control," *IEEE/ASME Transactions on Mechatronics* **20**(5), 2031–2038 (2015).
- <sup>11</sup> S. Zimmermann, T. Tiemerding, O. C. Haenssler, and S. Fatikow, "Automated robotic manipulation of individual sub-micro particles using a dual probe setup inside the scanning electron microscope," 2015 IEEE International Conference on Robotics and Automation, Washington State Convention Center Seattle, Washington, 950–955 (2015).
- <sup>12</sup> C. Ru, Y. Zhong, Y. Sun, Y. Zhong, X. Sun, D. Hoyle, and I. Cotton, "Automated four-point probe measurement of nanowires inside a scanning electron microscope," *IEEE Transactions on Nanotechnology* **10**, 674–681 (2011).
- <sup>13</sup> K. H. Ong, J. C. H. Phang, and J. T. L. Thong, "A robust focusing and astigmatism correction method for the scanning electron microscope," *Scanning* **19**, 553–563 (1997).
- <sup>14</sup> J. Vargas, J. Oton, R. Marabibi, S. Jonic, J. M. de la Rosa-Trevin, J. M. Carazo, and C. O. S. Sorzano, "FASTDEF: Fast defocus and astigmatism estimation for high-throughput transmission electron microscopy," *Journal of Structural Biology* **181**, 136–148 (2013).
- <sup>15</sup> C. O. S. Sorzano, S. Jonic, R. Nunez-Ramirez, N. Boisset, and J. M. Carazo, "Fast, robust, and accurate determination of transmission electron microscopy contrast transfer function," *Journal of Structural Biology* **160**, 249–262 (2007).
- <sup>16</sup> H. C. Kan, D. Auerbach, and R. J. Phaneuf, "Approach for investigating the astigmatism of a magnetic prism in a low-energy electron microscopy," *Review of Scientific Instruments* **74**(2), 1008–1015 (2003).
- <sup>17</sup> R. E. Burge, M. T. Browne, J. C. Dainty, M. Derome, and S. Lackovic, "High resolution with STEM," Proc 6<sup>th</sup> Europ Congr Electron Microscopy, 1: 442–444 (1976).
- <sup>18</sup> W. J. Tee, K. C. A. Smith, and D. M. Holbium, "An automatic focusing and stigmating system for the SEM," *J. Phys. E: Science Instrument* **12**, 35–38 (1979).
- <sup>19</sup> S. J. Erasmus and K. C. A. Smith, "An automatic focusing and astigmatism correction system for the SEM and CTEM," *Journal of Microscope* **127**, 185–199 (1982).
- <sup>20</sup> J. H. Ahn, T.-W. Kim, and H. J. Pahk, "Fast focus and astigmatism correction algorithm for critical dimension measurement using electron microscopy," *International Journal of Precision Engineering and Manufacturing* **16**, 1941–1947 (2015).
- <sup>21</sup> B. Yan, B. Wang, and Y. Li, "Optical ellipse fitting method based on least square principle," *Journal of Beijing University of Aeronautics and Astronautics* **03**, 295–298 (2008).
- <sup>22</sup> R. Chen and Y. Sun, "The study of an improved randomized algorithm for detecting ellipses based on least square approach," *Industrial Instrumentation and Automation* **02**, 35–38 (2017).
- <sup>23</sup> F. Xiong, X. Li, and X. Han, "A method of ellipse fitting based on total least squares," *Microelectronics & Computer* **34**, 102–105 (2017).
- <sup>24</sup> M. Liao, Y. Zhao, Y. Zeng, Z. Huang, B. Zhang, and B. Zou, "Automatic segmentation for cell images based on support vector machine and ellipse fitting," *Journal of Zhejiang University* **51**(4), 722–728 (2017).
- <sup>25</sup> W. D. Riecke, "Practical lens design," *Topics in Current Physics: Magnetic Electron Lenses* (Spring-Verlag, 1982), pp. 164–135.